1-25-2005

Carbon-Based Ocean Productivity and Phytoplankton Physiology from Space

M. J. Behrenfeld

Emmanuel Boss
University of Maine - Main, emmanuel.boss@maine.edu

D. A. Siegel

D. M. Shea

Carbon-based ocean productivity and phytoplankton physiology from space

Michael J. Behrenfeld,[1,2] Emmanuel Boss,[3] David A. Siegel,[4] and Donald M. Shea[5]

Received 21 May 2004; revised 19 October 2004; accepted 2 November 2004; published 25 January 2005.

[1] Ocean biogeochemical and ecosystem processes are linked by net primary production (NPP) in the ocean's surface layer, where inorganic carbon is fixed by photosynthetic processes. Determinations of NPP are necessarily a function of phytoplankton biomass and its physiological status, but the estimation of these two terms from space has remained an elusive target. Here we present new satellite ocean color observations of phytoplankton carbon (C) and chlorophyll (Chl) biomass and show that derived Chl:C ratios closely follow anticipated physiological dependencies on light, nutrients, and temperature. With this new information, global estimates of phytoplankton growth rates (μ) and carbon-based NPP are made for the first time. Compared to an earlier chlorophyll-based approach, our carbon-based values are considerably higher in tropical oceans, show greater seasonality at middle and high latitudes, and illustrate important differences in the formation and demise of regional algal blooms. This fusion of emerging concepts from the phycological and remote sensing disciplines has the potential to fundamentally change how we model and observe carbon cycling in the global oceans.

Citation: Behrenfeld, M. J., E. Boss, D. A. Siegel, and D. M. Shea (2005), Carbon-based ocean productivity and phytoplankton physiology from space, *Global Biogeochem. Cycles*, *19*, GB1006, doi:10.1029/2004GB002299.

1. Introduction

[2] Marine net primary production (NPP: mg C m^{-2}) is a key metric of ecosystem health and carbon cycling and is commonly estimated as the product of plant biomass, incident solar flux, and a scaling parameter that accounts for variations in plant physiology [*Behrenfeld et al.*, 2001]. Satellite measurements now routinely provide global chlorophyll biomass (Chl) and incident light (I_0) data, but the remote determination of phytoplankton carbon (C) biomass and physiological status has proven elusive. Present-day ocean NPP estimates consequently use chlorophyll as an index of phytoplankton biomass and rely on stylized empirical descriptions of physiological variability [e.g., *Longhurst*, 1995; *Behrenfeld and Falkowski*, 1997a] that perform poorly when compared to local field measurements [*Siegel et al.*, 2001; *Campbell et al.*, 2002; *Behrenfeld et al.*, 2002]. Far more is known, however, regarding the nature of phytoplankton physiology than is reflected in these empirical relationships. In particular, laboratory studies have long shown that phytoplankton respond to changes in light, nutrients, and temperature conditions by adjusting cellular pigment levels to match their new demands for photosynthesis and that this response is well quantified by changes in the ratio of chlorophyll to carbon biomass (Chl:C) [e.g., *Geider*, 1987; *Sakshaug et al.*, 1989; *MacIntyre et al.*, 2002]. It follows, therefore, that a remote sensing index of Chl:C may provide a path for assessing phytoplankton physiology from space.

[3] Optical scattering coefficients in marine waters covary with the suspended particle load (see review by *Babin et al.* [2003]). Indeed, the particulate beam attenuation coefficient at 660 nm (c_p) (an inherent optical property that is dominated by scattering) has been repeatedly shown in the field to covary with the particulate organic carbon concentration (POC) [*Gardner et al.*, 1993, 1995; *Walsh et al.*, 1995; *Loisel and Morel*, 1998; *Bishop*, 1999; *Bishop et al.*, 1999; *Claustre et al.*, 1999]. *Behrenfeld and Boss* [2003] suggested that c_p should likewise be well correlated with phytoplankton carbon biomass, particularly since the particle size domain dominating c_p more closely matches that of phytoplankton than POC. Accordingly, they proposed the c_p:Chl ratio as an index of phytoplankton C:Chl and subsequently demonstrated a first-order correspondence between c_p:Chl and independent ^{14}C-tracer measures of physiological condition [*Behrenfeld and Boss*, 2003]. Thus the ratio of chlorophyll to light scattering appears to provide an optical index of phytoplankton physiology.

[4] Currently, c_p is not a remote sensing product. However, recent advances in satellite ocean color data analysis now permit the separation of light absorbing and scattering components in seawater, yielding simultaneous estimates of Chl and particulate backscattering coefficients (b_{bp}) [*Maritorena*

[1]National Aeronautic and Space Administration, Goddard Space Flight Center, Greenbelt, Maryland, USA.
[2]Now at Department of Botany and Plant Pathology, Oregon State University, Corvallis, Oregon, USA.
[3]School of Marine Sciences, University of Maine, Orono, Maine, USA.
[4]Institute for Computational Earth System Science, University of California, Santa Barbara, California, USA.
[5]Science Applications International Corporation, NASA Goddard Space Flight Center, Greenbelt, Maryland, USA.

0886-6236/05/2004GB002299

et al., 2002; *Siegel et al.*, 2002; *Stramski et al.*, 1999; *Loisel et al.*, 2001]. While b_{bp} is likely more influenced by particles outside the phytoplankton size domain than c_p [*Morel and Ahn*, 1991; *Stramski and Kiefer*, 1991], a relationship between b_{bp} and phytoplankton carbon is nevertheless anticipated so long as the abundance of non-algal particles contributing to b_{bp} covaries with phytoplankton biomass. Such covariability in components of the particle assemblage is evidenced by the relatively constant slope of the particle size spectrum in open ocean waters [*Bader*, 1970; *Stramski and Kiefer*, 1991; *Kiefer and Berwald*, 1992] (see also discussion by *Twardowski et al.* [2001]) and is responsible for reported correlations between satellite b_{bp} and field measurements of POC [*Stramski et al.*, 1999; *Loisel et al.*, 2001].

[5] Here we proceed through a sequence of steps that lead from satellite Chl and b_{bp} determinations to global carbon-based estimates of ocean NPP. From b_{bp}, we estimate phytoplankton carbon biomass (C) and then demonstrate that regional satellite Chl:C ratios behave in a manner consistent with well-established physiological dependencies on light, nutrients, and temperature. We then use Chl:C data to estimate phytoplankton growth rates (μ) and, finally, calculate NPP from the product of μ and C. In this manner, closure on the productivity equation is achieved through remote sensing, yielding a new view of global ocean productivity and its variation over space and time.

2. Methods

2.1. Global Data

[6] Chlorophyll concentrations (Chl: mg m^{-3}) and b_{bp} at 440 nm (m^{-1}) were estimated using the Garver-Siegel-Maritorena (GSM) semi-analytical algorithm [*Garver and Siegel*,1997; *Maritorena et al.*, 2002; *Siegel et al.*, 2002] and monthly satellite water-leaving radiances for the September 1997 to January 2002 period from the fourth reprocessing of the Sea-viewing Wide Field-of-view Sensor (SeaWiFS) data set. The GSM algorithm provides chlorophyll products that compare equally well with coincident open ocean observations as chlorophyll products from the standard SeaWifs algorithm (D. M. Siegel et al., Independence and interdependences of global ocean optical properties viewed using satellite color imagery, submitted to *Journal of Geophysical Research*, 2004). For this analysis, we also used coincident SeaWiFS cloud-corrected surface PAR data (I_0: moles photons m^{-2} h^{-1}), SeaWiFS mixed layer light attenuation coefficients at 490 nm (k_{490}: m^{-1}), 8-km advanced very high resolution radiometer (AVHRR) sea surface temperature data (SST; °C) from the Physical Oceanography Distributed Active Archive Center (PODAAC) (http://podaac-www.jpl.nasa.gov), and monthly mean regional mixed layer depths (MLD: m) from the Fleet Numeric Meteorology and Oceanography Center (FNMOC) (Monterey, California). While FNMOC and climatological MLD data compare favorably over large space scales and timescales, the FNMOC model assimilates coincident field and satellite temperature and salinity data and thus provides information on interannual variability in MLDs. I_0, k_{490}, and MLD data were used to calculate monthly median mixed layer light levels (I_g) following: $I_g = I_0 \exp^{-k490 \times MLD/2}$.

2.2. Regional Binning

[7] Arctic and coastal regions were excluded from our analysis, and the remaining data (89% of the global oceans) were partitioned into 28 regional bins, defined by ocean basin and the degree of seasonal variability in chlorophyll. Standard deviations in Chl ($s.d._{Chl}$) provide a means to coarsely separate functionally different ocean regions (e.g., oligotrophic versus seasonal bloom areas) [*Esaias et al.*, 1999; *Doney et al.*, 2003]. For the current study, five chlorophyll variance bins (L0 to L4) were used and defined as: L0 = $0 < s.d._{Chl} < 0.018$ mg Chl m^{-3}, L1 = $0.018 < s.d._{Chl} < 0.026$ mg Chl m^{-3}, L2 = $0.026 < s.d._{Chl} < 0.09$ mg Chl m^{-3}, L3 = $0.09 < s.d._{Chl} < 0.4$ mg Chl m^{-3}, and L4 = $s.d._{Chl} > 0.4$ mg Chl m^{-3}. The precise cutoff values for these bins are not critical and were simply chosen to yield regions consistent with large-scale ocean circulation and pigment features. All data for the Southern Ocean were grouped into a single bin because >90% of the data fell into L2 and L3 variance levels and the seasonal patterns in these bins were nearly identical.

2.3. Phytoplankton Carbon

[8] To constrain our satellite-based phytoplankton carbon estimates, we analyzed laboratory data compiled by *Behrenfeld et al.* [2002] on light- and nutrient-dependent changes in cellular pigmentation from published studies between 1946 and 1987. This data set yielded Chl:C values ranging from 0.001 to >0.06 mg mg^{-1}, with a median value of 0.010 mg mg^{-1} for light levels between 0.7 and 1.4 moles photons m^{-2} h^{-1}. The median mixed layer I_g for our remote sensing data set was 1.2 moles photons m^{-2} h^{-1}.

[9] As an additional constraint, satellite-based POC concentrations were calculated from b_{bp} data as the average of relationships developed for the Mediterranean (POC = 37550 $b_{bp}(550)$ + 1.3 = 29769 $b_{bp}(440)$ + 1.3) [*Loisel et al.*, 2001] and the Antarctic Polar Front Zone (POC = 17069 $b_{bp}(510)^{0.859}$ = 14726 $b_{bp}(440)^{0.859}$) [*Stramski et al.*, 1999], where the first equation is the original published relationship and the second equation is the converted relationship for use with $b_{bp}(440)$ data. We then calculated phytoplankton carbon:POC ratios for our remote sensing data and compared these to field-derived values. Specifically, *Eppley et al.* [1992] reported phytoplankton carbon:POC ratios of 29% to 49%, *DuRand et al.* [2001] found a relatively constant value of 33% throughout the year near Bermuda, *Gundersen et al.* [2001] reported a value of 32%, and *Oubelkheir* [2001] measured values ranging from 19% to 21% in regions spanning from oligotrophic to eutrophic. It is noteworthy that this restricted variability observed in the field includes methodological differences for estimating phytoplankton carbon.

2.4. Productivity Calculations

[10] For comparative purposes, global ocean NPP was calculated using our new carbon-based approach and a

common chlorophyll-based algorithm, the Vertically Generalized Production Model (VGPM) [*Behrenfeld and Falkowski*, 1997a]. The depth-integrated VGPM equation is NPP = Chl × Z_{eu} × $f(I_0)$ × d.l. × P^b_{opt}, where Z_{eu} is the depth of the photosynthetically active surface layer and physiological variability (P^b_{opt}) is described by an empirical polynomial function of SST that increases from 0° to 20°C and then decreases at higher temperatures [*Behrenfeld and Falkowski*, 1997a]. For both the chlorophyll- and carbon-based calculations, the light-dependent function was described as, $f(I_0) = 0.66125\ I_0/(I_0 + 4.1)$ [*Behrenfeld and Falkowski*, 1997a], Z_{eu} was calculated as $Z_{eu} = \ln(0.01)/k_{490}$ (which gives slightly higher NPP values than earlier VGPM estimates), and the same GSM satellite chlorophyll estimates were used.

3. Results

3.1. Satellite-Based Phytoplankton Carbon Biomass

[11] Comparison of monthly b_{bp} and Chl data revealed two distinct regimes: one where b_{bp} is relatively constant and one where b_{bp} covaries with Chl (Figure 1). In the most unproductive ocean regions, b_{bp} varies by only a factor of 1.6 (from 0.0010 to 0.0016 m^{-1}) while Chl ranges from 0.03 to 0.14 mg m^{-3} (i.e., a factor of 4.6), with no correlation between the two variables (Figure 1). In more productive regions where chlorophyll concentrations exceed ~0.14 mg Chl m^{-3}, b_{bp} and Chl are well correlated (r^2 = 0.74) (Figure 1). Our interpretation of this bilinear pattern is that Chl variability is largely due to intracellular changes in pigmentation (i.e., physiology) in impoverished ocean regions, while in more enriched regions, first-order changes in Chl and b_{bp} are predominantly due to changes in phytoplankton biomass (i.e., abundance).

[12] To estimate phytoplankton carbon biomass (mg m^{-3}) from b_{bp}, we first subtracted a background value of 0.00035 m^{-1} and then multiplied by a scalar of 13,000 mg C m^{-2} (i.e., phytoplankton C = 13,000 × (b_{bp} − 0.00035)). The background value was estimated from least squares regression analysis of the linear portion of the Chl-b_{bp} relationship (Figure 1, solid line), and it represents a global estimate of backscattering by the stable heterotrophic and detrital components of the surface particle population. For comparison, a similar independent estimate of 0.00017 m^{-1} is calculated using backscattering coefficients from *Stramski and Kiefer* [1991] and a field-based background heterotrophic bacterial concentration of 7 × 10^{11} m^{-3} from *Cho and Azam* [1990, Figure 1]. The scalar of 13,000 mg C m^{-2} was chosen to give satellite Chl:C values (average = 0.010, range = 0.002 to 0.030) consistent with laboratory results and an average phytoplankton contribution to total particulate organic carbon of ~30% (range: 24% to 37%), which is consistent with field estimates from a variety of ocean regions [*Eppley et al.*, 1992; *DuRand et al.*, 2001; *Gundersen et al.*, 2001; *Oubelkheir*, 2001] (see section 2.3).

[13] Restating the above in more general terms, we assume that the particle population contributing to b_{bp} is comprised of a stable non-algal "background" component and a second component that includes phytoplankton and other particles that covary with phytoplankton. We then subtract the "background" component and directly relate the remaining b_{bp} to phytoplankton biomass using a simple scalar that gives reasonable values for both Chl:C and the phytoplankton carbon to POC ratio. We do not assume that the remaining b_{bp} is entirely due to backscattering by phytoplankton, only that it correlates with phytoplankton abundance. This conversion of b_{bp} to phytoplankton carbon will clearly be compromised by significant shifts in the composition of the particle assemblage (e.g., prominent inorganic particulate component) or by large deviations in the slope of the particle size spectrum. The influence of local-scale variability in such factors has been minimized in the current analysis by integrating monthly data over large areas and omitting coastal waters where suspended inorganic particle loads can be particularly high (see section 2.2).

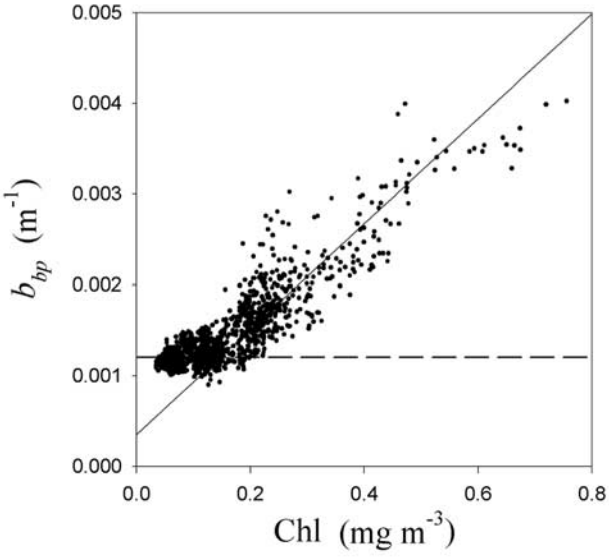

Figure 1. Regional monthly mean particulate backscattering coefficients at 440 nm (b_{bp}) and surface chlorophyll concentrations (Chl) for the September 1997 to January 2002 period. Data are from the 28 regional bins identified in Figure 2a. The solid line represents a linear fit to data with Chl > 0.14 mg m^{-3}. The dashed line indicates the mean b_{bp} value of 0.0012 m^{-1} for data where Chl < 0.14 mg m^{-3} (i.e., the realm where Chl and b_{bp} are uncorrelated).

[14] In the next two sections, we describe how regional variability in satellite Chl:C is consistent with anticipated changes in phytoplankton physiology. Importantly, these results are quite insensitive to the b_{bp}-to-carbon conversion parameters described above, such that the same degree of correspondence with mixed layer growth conditions is found with unaltered Chl:b_{bp} ratios as with our converted Chl:C values.

3.2. Five Basic Seasonal Patterns in Phytoplankton Biomass and Physiology

[15] Analysis of regional phytoplankton Chl, C, and Chl:C ratios revealed seasonal patterns related to basic

ocean circulation and ecosystem features. Parallel changes in Chl and C biomass reflect changes in phytoplankton abundance caused by shifts in the balance between phytoplankton growth and losses (e.g., sinking, predation). Divergent patterns in Chl and C (i.e., changes in the Chl:C ratio) result from physiological acclimations to changing growth conditions. Quite specifically, decreases in Chl:C are associated with increases in growth irradiance (I_g), decreases in nutrients, and decreases in temperature [*Geider*, 1987; *Sakshaug et al.*, 1989; *Cloern et al.*, 1995; *Geider et al.*, 1998; *MacIntyre et al.*, 2002; *Behrenfeld et al.*, 2002].

[16] From our 28 regions, five basic seasonal patterns emerged (Figure 2) (see the REGPAT figures in the auxiliary material[1] for all 28 regional graphs). In eight of the lowest production regions (see Figure 2 caption), stable environmental conditions foster stable C concentrations through a tight coupling between phytoplankton growth and consumption, while seasonal changes in light cause smooth seasonal cycles in Chl, and thus Chl:C (Figure 2b). In other words, phytoplankton biomass is essentially constant throughout the year in these unproductive waters, but chlorophyll still varies notably from physiological responses to seasonally changing growth conditions (i.e., intracellular chlorophyll increases during winter months in response to generally deeper mixed layers, lower light levels, and possibly higher nutrient levels [*Winn et al.*, 1995; *McClain et al.*, 2004]). In four other low production regions, the coupling between phytoplankton growth and consumption is not so tight, and this imbalance causes moderate changes in C and Chl biomass (Figure 2c). Physiological responses to changing light and nutrient stress in these regions cause additional variability in Chl that leads to somewhat dampened Chl:C cycles with both spring and fall peaks (Figure 2c). Together, these 12 regions contribute most of the Chl-b_{bp} pairs in Figure 1 at <0.14 mg Chl m^{-3}, where chlorophyll variability is predominantly due to changes in physiological state.

[17] In five moderately productive regions, temporally offset seasonal cycles of Chl and C biomass are found, with the rise in Chl preceding the rise in C (Figure 2d). We interpret this pattern as a seasonal cycle where initial cell "greening" is followed by increased growth and biomass, and later culminates in nutrient- and light-dependent reductions in pigmentation and growth. Nine other moderate- and high-production areas exhibit seasonal cycles in both Chl and C biomass that are dominated by large spring-summer blooms in phytoplankton abundance (Figure 2e). Despite this first-order influence of biomass, physiological adjustments during the seasonal cycle are still registered by coherent second-order changes in Chl:C ratios that increase during low-light and early bloom conditions and decrease just prior to the biomass peak and crash (Figure 2e). These qualitative results thus indicate that scatter in the Chl-b_{bp} relationship at >0.14 mg Chl m^{-3} (Figure 1) is indeed associated with seasonal changes in phytoplankton physiology.

[18] The fifth temporal pattern revealed by this analysis was unique to the two equatorial upwelling regions of the central Pacific (i.e., CP-L2, CP-L3 (Figure 2a)) and characterized by a strong shift in Chl:C during the 1997–1998 El Niño to La Niña transition [*Chavez et al.*, 1999; *Behrenfeld et al.*, 2001], followed by an extended period of low-level, correlated variability in Chl and C (Figure 2f). This pattern is consistent with the regions' low amplitude variability in mixing depths and surface light (therefore, I_g) and the dominating influence of El Niño-La Niña shifts in nutrient availability on phytoplankton physiology (Figure 2f).

3.3. Satellite-Derived Physiology Registers Light, Nutrient, and Temperature Effects

[19] It is well established from decades of laboratory studies that phytoplankton Chl:C ratios decrease from low to high light [e.g., *Geider*, 1987; *Sakshaug et al.*, 1989; *Geider et al.*, 1998; *MacIntyre et al.*, 2002; *Behrenfeld et al.*, 2002]. This phenomenon, known as "photoacclimation," reflects physiological responses aimed at minimizing the influence of light variability on growth (Figure 3a). The relationship between Chl:C and light has a low-light maximum (Chl:C_{max}) that increases with increasing temperature [*Geider*, 1987; *Cloern et al.*, 1995] (Figure 3b) and a light-saturated minimum (Chl:C_{min}) that decreases with increasing nutrient stress [*Laws and Bannister*, 1980; *Sakshaug et al.*, 1989; *Cloern et al.*, 1995; *Geider et al.*, 1998] (Figure 3c). These adjustments in cellular pigmentation function to balance light harvesting with temperature- and nutrient-dependent changes in growth. The dependency of Chl:C on light can be modeled for a range of growth conditions as an exponential function of light [*Cloern et al.*, 1995; *Behrenfeld et al.*, 2002], such as

$$\mathrm{Chl:C} = \mathrm{Chl:C_{min}} + [\mathrm{Chl:C_{max}} - \mathrm{Chl:C_{min}}]\exp^{-3\,\mathrm{Ig}}. \quad (1)$$

[20] To more quantitatively link satellite Chl:C data with phytoplankton physiology, we compared regional changes in Chl:C with corresponding changes in mixed layer light levels (I_g) and found clear relationships that closely followed equation (1) (median $r = 0.85$) in all regions with significant seasonal variability in I_g (Figure 3d) (Table 1). In other words, regional Chl:C values varied with I_g precisely as expected from the laboratory (compare Figures 3a and 3d). Overall, equation (1) captured 94% of the global variability in satellite Chl:C. Moreover, fits of equation (1) to the regional Chl:C data yielded Chl:C_{max} values that increased with increasing sea surface temperature (SST) ($r^2 = 0.79$) in a manner consistent with laboratory trends [*Geider*, 1987; *Cloern et al.*, 1995] (Figure 3e). Differences of scale in these relationships indicate that the nutrient-saturated, exponential growth conditions used in laboratory monoculture studies (Figures 3a and 3b) are rarely replicated for all members of any natural phytoplankton community (Figures 3d and 3e).

[21] While nutrient concentrations are not directly measured from space, the global tendency is for surface nutrients to decrease with increasing SST [*Kamykowski et al.*, 2002; *Switzer et al.*, 2003]. Accordingly, we found

[1] Auxiliary material is available at ftp://ftp.agu.org/apend/gb/2004GB002299.

that fits of equation (1) yielded regional values for the nutrient-dependent term, Chl:C_{min}, that decreased with increasing SST in 21 of our 28 regions ($r^2 = 0.83$) (Figure 3f, solid circles). The seven remaining regions were all areas where SST is a poor surrogate for nutrient stress. For the six high-temperature outliers (Figure 3f, open triangles), equatorial or monsoon-driven upwelling sustains elevated nutrients and productivity. In these regions, annual mean

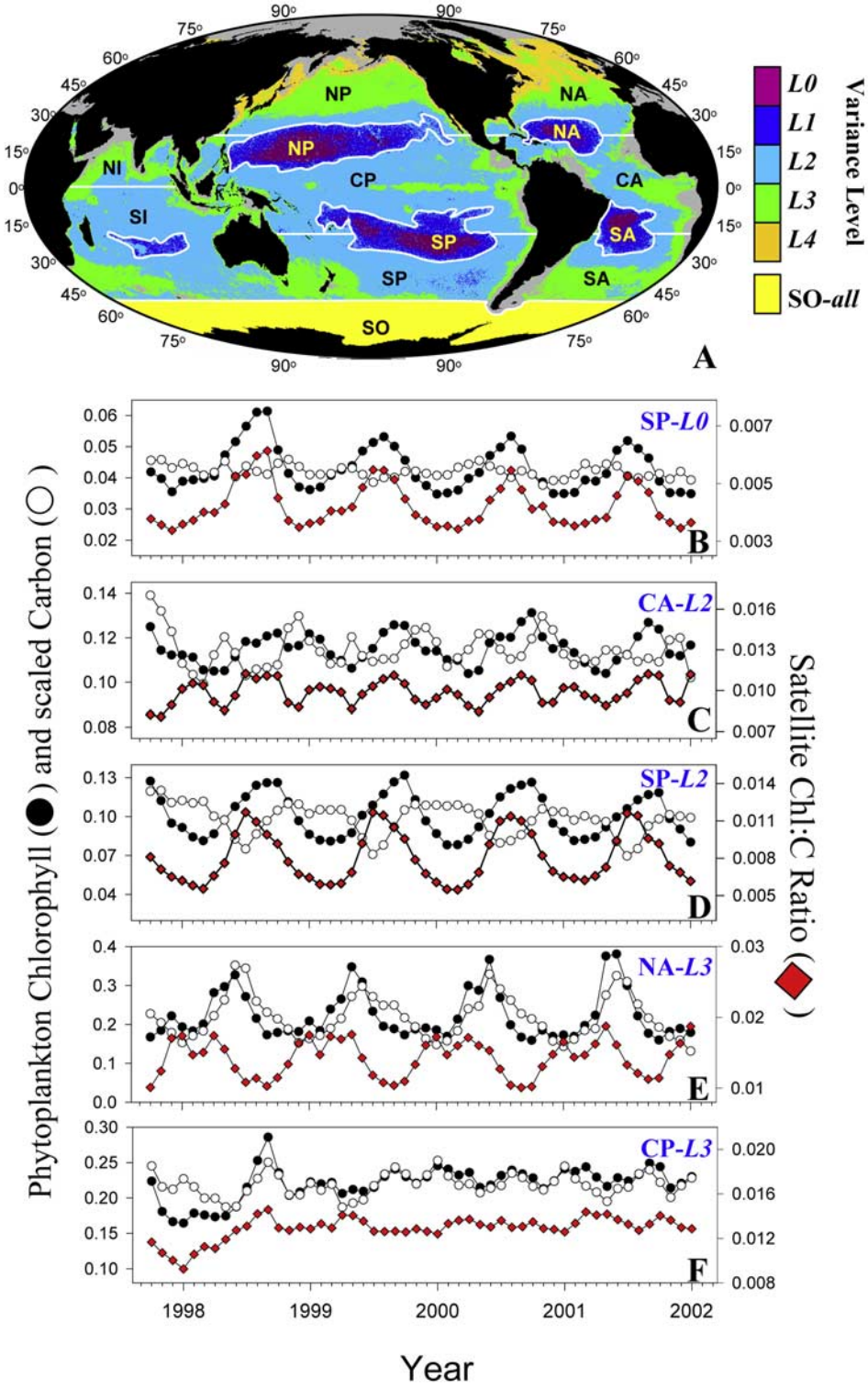

Figure 2

Chl is a more robust index of nutrient input and indeed is well correlated with Chl:C_{min} ($r^2 = 0.93$). The single low temperature outlier (Figure 3f, open circle) corresponds to the Southern Ocean region, where macronutrients (NO_3, PO_4) are abundant, but phytoplankton growth is limited by iron availability and temperature (annual mean = 1.6°C).

[22] Analysis of our satellite Chl:C data thus reveals (1) seasonal patterns consistent with regional ecology (Figures 2b–2f), (2) strong dependencies on mixed layer light levels (median $r = 0.85$) that are consistent with laboratory studies (compare Figures 3a with 3d), and (3) estimates of Chl:C_{max} and Chl:C_{min} that follow anticipated relationships with SST (compare Figures 3b and 3c with 3e and 3f) and have minimum values (0.0155 and 0.0037, respectively) (Figures 3e and 3f) indistinguishable from laboratory-based estimates (0.0154 and 0.0030, respectively) [*Cloern et al.*, 1995]. Taken together, these findings strongly support a link between satellite Chl:C and phytoplankton physiology, and thus a path from ocean color to phytoplankton growth rates (μ).

3.4. Phytoplankton Growth Rates From Space

[23] The growth rate of a natural phytoplankton community (μ: divisions d^{-1}) is a function of light, nutrients, and temperature and can be described by

$$\mu = \mu_{max} \times f(N,T) \times g(I_g), \quad (2)$$

where, f(N, T) accounts for reductions in growth rate due to nutrient and temperature limitation at a given light level (range: 0 to 1), $g(I_g)$ accounts for reductions in growth rate due to light limitation (range: 0 to 1), and μ_{max} is the maximum potential community growth rate under optimal conditions. Equation (2) is applied here to estimate community carbon-specific phytoplankton growth rates and does not provide information on growth of specific algal groups (e.g., the bulk growth rate of an oligotrophic community may be low despite a picoplankton fraction dividing nearly once per day).

[24] As a first attempt at estimating μ from satellite Chl:C data, we assigned μ_{max} a value of 2 divisions d^{-1}, based on the highest phytoplankton community growth rates reported in the extensive field data set compiled by *Banse* [1991]. We then assumed that increases in nutrient and temperature stress cause decreases in phytoplankton growth rates that are paralleled by proportional decreases Chl:C ratios [*Geider*, 1987; *Sakshaug et al.*, 1989; *Cloern et al.*, 1995]. This response (which is the f (N, T) function in equation (2)) was quantified by dividing satellite Chl:C data (Chl:C_{sat}) by a maximum potential community chlorophyll:carbon value for a given I_g (Chl:$C_{N,T\text{-}max}$),

$$\mu = \mu_{max} \times \left[\mathrm{Chl:C_{sat}}/\mathrm{Chl:C_{N,T\text{-}max}}\right] \times g(I_g). \quad (3)$$

Chl:$C_{N,T\text{-}max}$ was then defined by a parameterization of equation (1) that enveloped >99% of our satellite Chl:C data, specifically: Chl:$C_{N,T\text{-}max} = 0.022 + (0.045 - 0.022)\exp^{-3Ig}$ (Figure 4a, blue line). This description of Chl:$C_{N,T\text{-}max}$ has a Chl:C_{min} value (0.022) that is somewhat higher than the fitted curves for our 28 regions (Figure 4a), implying that high light environments are generally associated with suboptimal growth conditions at the regional scale (note that at the pixel scale, near-maximum values are frequently observed). Finally, decreases in μ at low light result because physiological adjustments in pigmentation are insufficient to maintain constant levels of light absorption [*Geider*, 1987; *Sakshaug et al.*, 1989; *Cloern et al.*, 1995; *Geider et al.*, 1998]. With the dependence of Chl:C on I_g described by (1), this relationship between μ and light is given by $g(I_g) = 1 - \exp^{-3Ig}$. In summary, μ was estimated as

$$\mu = 2 \times \mathrm{Chl:C_{sat}}/\left[0.022 + (0.045 - 0.022)\exp^{-3Ig}\right] \times \left(1 - \exp^{-3Ig}\right). \quad (4)$$

Equation (4) was then applied uniformly to all 28 regions, including the seven outliers identified in Figure 3f (since these regions correspond to areas where SST is not a good predictor of nutrient stress, while Chl:C still tracks changes in physiology).

[25] Representing the first direct estimates of μ from space, we found mixed layer phytoplankton growth rates

Figure 2. (a) The 28 regional bins determined by ocean basin and chlorophyll variance. Variance levels (L0 to L4) are indicated by color. Low-production, central ocean gyres with the lowest chlorophyll variance (L0, L1) are outlined in white and separated into northern and southern components. All variance levels in the Indian Ocean are also separated into northern and southern components. Moderate to high variance levels (L2 to L4) in the Atlantic and Pacific are separated into northern, central, and southern components. A single bin was used for all Southern Ocean data (see section 2). Basin designations are: NA, North Atlantic; CA, Central Atlantic; SA, South Atlantic; NP, North Pacific; CP, Central Pacific; SP, South Pacific; NI, North Indian; SI, South Indian; SO, Southern Ocean. Black denotes land. Gray denotes Arctic and coastal areas not included. Figures 2b–2f give examples of the five basic temporal patterns in regional phytoplankton chlorophyll (Chl; solid circles) and carbon (C; open circles) biomass and Chl:C ratios (red diamonds; mg mg^{-1}). Left axis is Chl and C concentration (mg m^{-3}), where C has been multiplied by the following values to scale with chlorophyll: Figure 2b, 0.004; Figure 2c, 0.008; Figure 2d, 0.010; Figure 2e, 0.014; Figure 2f, 0.013. Right axis is Chl:C (mg mg^{-1}). (b) Pattern observed in regions NA-L0, NA-L1, NA-L2, SA-L1, NP-L2, SP-L0, SP-L1, SI-L1. (c) Pattern in regions CA-L2, SA-L0, NP-L0, NP-L1. (d) Pattern in regions SA-L2, SP-L2, SP-L3, SI-L2, SI-L3. (e) Pattern in regions NA-L3, NA-L4, CA-L3, SA-L3, NP-L, NP-L4, NI-L2, NI-L3, SO. (f) Pattern in regions CP-L2, CP-L3. The specific region shown is indicated at the top right: SP-L0 in Figure 2b, CA-L2 in Figure 2c, SP-L2 in Figure 2d, NA-L3 in Figure 2e, and CP-L3 in Figure 2f. Please refer to the REGPAT figures in the auxiliary material to view Chl, C, and Chl:C time series for all 28 regions.

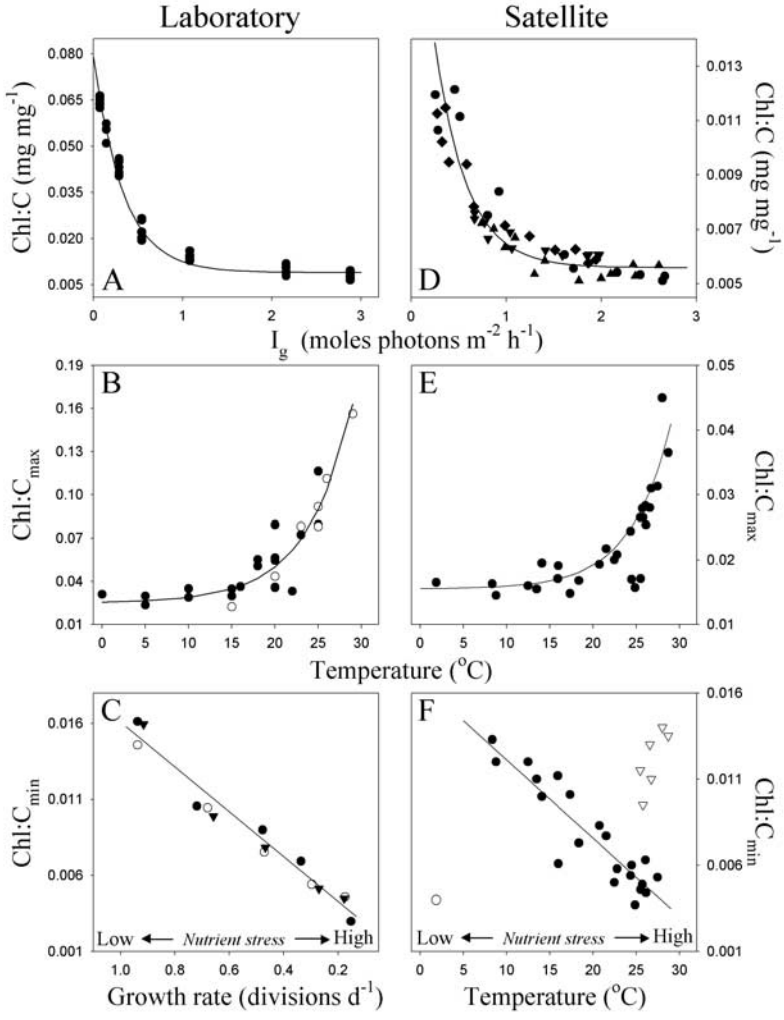

Figure 3. Changes in phytoplankton Chl:C ratios in response to changes in light, nutrients, and temperature as (Figures 3a–3c) observed in the laboratory and (Figures 3d–3f) derived from satellite ocean color data. (a) Chl:C values measured in monocultures of the marine chlorophyte, *Dunaliella tertiolecta*, grown over a range of light levels (I_g) at 20°C and with replete nutrients. (b) Temperature dependence of Chl:C_{max} for 16 cultured phytoplankton species as reported by *Geider* [1987]. Solid circles denote diatoms. Open circles denote all other species. (c) Influence of nutrient stress on Chl:C_{min} in the diatom, *Thalassiosira fluviatilis* [*Laws and Bannister*, 1980]. Nutrient stress is quantified by changes in growth rate (x axis). Solid circles denote NO_3 limited cultures. Open circles denote NH_4 limited cultures. Solid triangles denote PO_4 limited cultures. (d) Satellite Chl:C estimates versus I_g for four of the regions defined in Figure 2a. Solid circles denote SP-L1. Solid diamonds denote NA-L2. Solid upside-down triangles denote SP-L2. Solid right-side-up triangles denote SA-L1. Fitted curves for all 28 regions are shown in Figure 4a, and fit statistics are provided in Table 1. (e) Relationship between sea surface temperature (SST: °C) and fitted values of Chl:C_{max} for all 28 regions. Solid line denotes fit to data (Chl:C_{max} = 0.0155 + 0.00005 exp $^{0.215\ SST}$) (r^2 = 0.79). (f) Relationship between sea surface temperature (SST: °C) and fitted values of Chl:C_{min} for all 28 regions. Solid line denotes fit to solid circle data (Chl:C_{min} = 0.017 − 0.00045 SST) (r^2 = 0.83). Open triangles denote the six high-temperature outliers (L2 and L3 data from the North Indian, Central Pacific, Central Atlantic). Open circle denotes low-temperature outlier (Southern Ocean). These ''outliers'' are anticipated based on regional relationships between SST and constraints on phytoplankton growth (see text). Solid line in Figures 3a and 3d denotes fit of (1). Solid line in Figure 3b denotes fit of exponential model as in Figure 3e. Solid line in Figure 3c denotes linear regression fit to all data.

Table 1. Mean Surface Chlorophyll Biomass (mg m^{-3}), Mean Sea Surface Temperature (SST: °C), and Range in Median Mixed Layer Light Levels (I_g: Moles Photons m^{-2} h^{-1}) for Each Region (See Figure 2) During the September 1997 to January 2002 Period[a]

Region	Mean Chl Biomass	Mean SST	I_g Min–Max	Chl:C_{min}	Chl:C_{max}	Correlation Coefficients
			North Atlantic			
L0	0.053	26	0.85–2.51	0.0044	0.025	0.90
L1	0.060	26	0.82–2.3	0.0049	0.028	0.85
L2	0.091	23	0.26–2.67	0.0058	0.021	0.89
L3	0.226	16	0.01–1.61	0.0112	0.017	0.91
L4	0.413	8	<0.01–0.70	0.0133	0.016	0.65
			Central Atlantic			
L2	0.115	26	1.28–1.59	0.0095	0.027	0.67
L3	0.180	25	1.32–1.80	0.0115	0.027	0.72
			South Atlantic			
L0	0.054	25	0.73–2.30	0.0046	0.017	0.87
L1	0.063	24	0.74–2.60	0.0054	0.024	0.91
L2	0.113	18	0.20–1.91	0.0073	0.017	0.89
L3	0.254	12	0.04–0.74	0.0120	0.016	0.68
			North Pacific			
L0	0.060	27	1.09–1.67	0.0053	0.031	n.s.
L1	0.071	26	0.97–1.85	0.0063	0.028	0.48
L2	0.091	22	0.37–2.61	0.0077	0.022	0.91
L3	0.219	13	0.01–1.91	0.0110	0.016	0.67
L4	0.411	9	<0.01–0.37	0.0120	0.015	n.s.
			Central Pacific			
L2	0.130	27	1.10–1.50	0.0110	0.031	n.s.
L3	0.220	27	1.33–1.88	0.0130	0.028	n.s.
			South Pacific			
L0	0.043	24	0.68–2.38	0.0037	0.016	0.90
L1	0.072	24	0.67–1.98	0.0060	0.017	0.95
L2	0.101	16	0.27–1.94	0.0061	0.019	0.96
L3	0.213	14	0.09–1.37	0.0100	0.020	0.85
			North Indian			
L2	0.141	22	1.18–1.96	0.0135	0.037	0.67
L3	0.219	29	0.59–2.01	0.0140	0.045	0.94
			South Indian			
L1	0.061	28	0.62–2.60	0.0049	0.020	0.85
L2	0.128	21	0.32–1.90	0.0083	0.019	0.83
L3	0.211	17	0.09–1.19	0.0101	0.015	0.85
			Southern Ocean			
All	0.168	2	0.01–0.60	0.004	0.013	0.81

[a]Also provided is Chl:C_{min}, Chl:C_{max}, and correlation coefficients for regional fits of equation (1). Chl:C_{min} and Chl:C_{max} [mg Chl (mg C)$^{-1}$] are all significant at $p < 0.0005$; n.s. = not significant.

to be persistently elevated in the upwelling-enriched tropical oceans, chronically suppressed in the stratified central ocean gyres, and strongly seasonal at higher northern and southern latitudes (Figures 4b and 4c). In the equatorial Pacific, μ peaked along the upwelling axis near the equator and then diminished to the north and south (Figures 4b and 4c), as often suggested by field ^{14}C-uptake measurements [*Lindley et al.*, 1995; *Behrenfeld and Boss*, 2003]. At high southern latitudes where easterly circumpolar currents prevail, enhanced summertime growth rates were largely restricted to the leeward eastern margins of continents and islands (Figure 4c), consistent with sources of growth-limiting micronutrients (i.e., iron) [*Boyd et al.*, 1999; *Sullivan et al.*, 1993]. In the North Atlantic and western Pacific, spring and summer growth rates were broadly elevated across middle and high latitudes, reflecting a shoaling of surface mixing depths and elevated sunlight (Figure 4b). The markedly lower summer growth rates in the eastern subarctic Pacific are consistent with this region's restriction by iron availability [*Boyd et al.*, 1996; *Harrison et al.*, 1999] (Figure 4b). Globally, satellite-based phytoplankton community growth rates exhibited a smooth, peaked distribution with a median around 0.5 divisions d^{-1} (Figure 4d).

3.5. Global Ocean Productivity

[26] The product of phytoplankton carbon biomass and growth rate is net primary production. Water column NPP can be estimated from surface satellite C and μ by additionally accounting for changes in photosynthesis with depth,

$$\mathrm{NPP} = \mathrm{C} \times \mu \times Z_{eu} \times h(I_0), \quad (5)$$

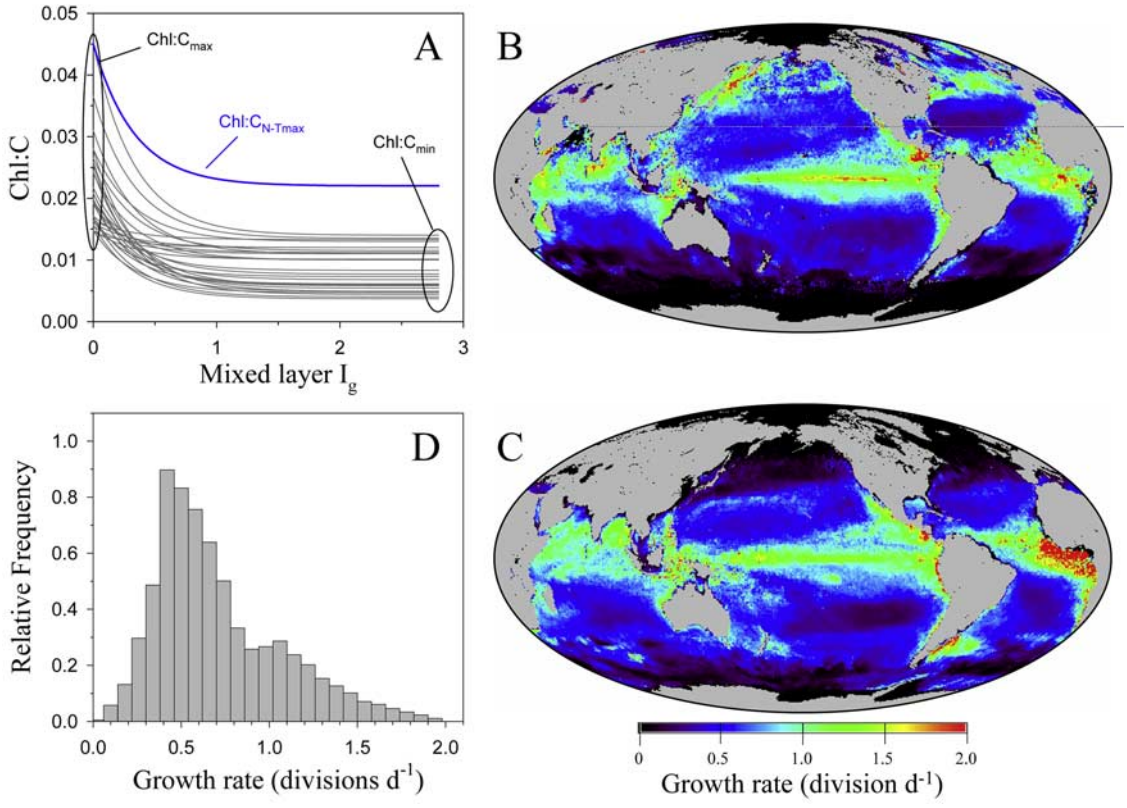

Figure 4. (a) Phytoplankton chlorophyll to carbon (Chl:C) ratios versus median mixed layer growth irradiance (I_g: moles photons m^{-2} h^{-1}). Blue line denotes modeled maximum Chl:C. Gray lines denote fits of (1) to the 28 regions (see Figure 2a). Figures 4b and 4c show seasonal mean mixed layer phytoplankton growth rates (μ: divisions d^{-1}) calculated from satellite Chl:C using (2). (b) Boreal summer (June to August). (c) Boreal winter (December to February). (d) Frequency histogram of annual mean satellite-based phytoplankton growth rates.

where Z_{eu} is the depth (m) of the photosynthetically active surface layer and $h(I_0)$ describes how changes in surface light influence the depth-dependent profile of carbon fixation. Equation (5) is of the same form as earlier NPP models [*Behrenfeld and Falkowski*, 1997b], with the exception that Chl is replaced by C and the empirical estimate of chlorophyll-specific photosynthesis (P^b_{opt}) is replaced by μ (where C and μ are now directly estimated from remote sensing; see above). To illustrate the impact of this new carbon-based approach, we now compare NPP calculated from (5) and a common Chl-based algorithm, the Vertically Generalized Production Model (VGPM) [*Behrenfeld and Falkowski*, 1997a] (see section 2.4).

[27] Annual total global ocean productivity averaged 67 Pg C yr^{-1} (Pg = 10^{15} g) for the C-based model and 60 Pg C yr^{-1} for the Chl-based model over the 1997 to 2002 period, a difference that scales directly with the value of μ_{max}. Far more striking (and independent of μ_{max}) are the spatial and seasonal differences in NPP between models (Figures 5a–5d). The carbon model yielded 40% and 49% higher annual NPP for the central Atlantic and central Pacific regions (see Figure 2 for regional boundaries) and an increase from 1.6 to 2.6 Pg C yr^{-1} in the north Indian region (Figures 5e and 5f). (It is interesting to note that the two models are in better agreement in these areas when an exponential model for P^b_{opt}, following *Antoine et al.* [1996], is used in the VGPM. This exponential expression performs better at low latitudes than the standard VGPM model based on comparisons with ^{14}C data [*Campbell et al.*, 2002].) Carbon-based NPP was also higher by 9% in the south Indian, 7% in the North Pacific, and 2% in the South Pacific regions (Figures 5e and 5f). The opposite trend was found for the North and South Atlantic, where NPP was 21% and 18% lower for the C model than the Chl model, respectively (Figures 5e and 5f). In the Southern Ocean, the relationship between C- and Chl-based NPP was patchy (particularly in summer months) (Figure 5f), but overall the C model gave a 20% lower estimate for this region.

[28] Without exception, the C-based and Chl-based models yielded different seasonal cycles in NPP, and often dramatically so (see the NPP figures in the auxiliary material to view time series for all 28 regions). While each region exhibited unique differences, the general trend over variance levels was for the C model to give dampened cycles relative to the Chl model in low variance regions, and often stronger and delayed seasonal

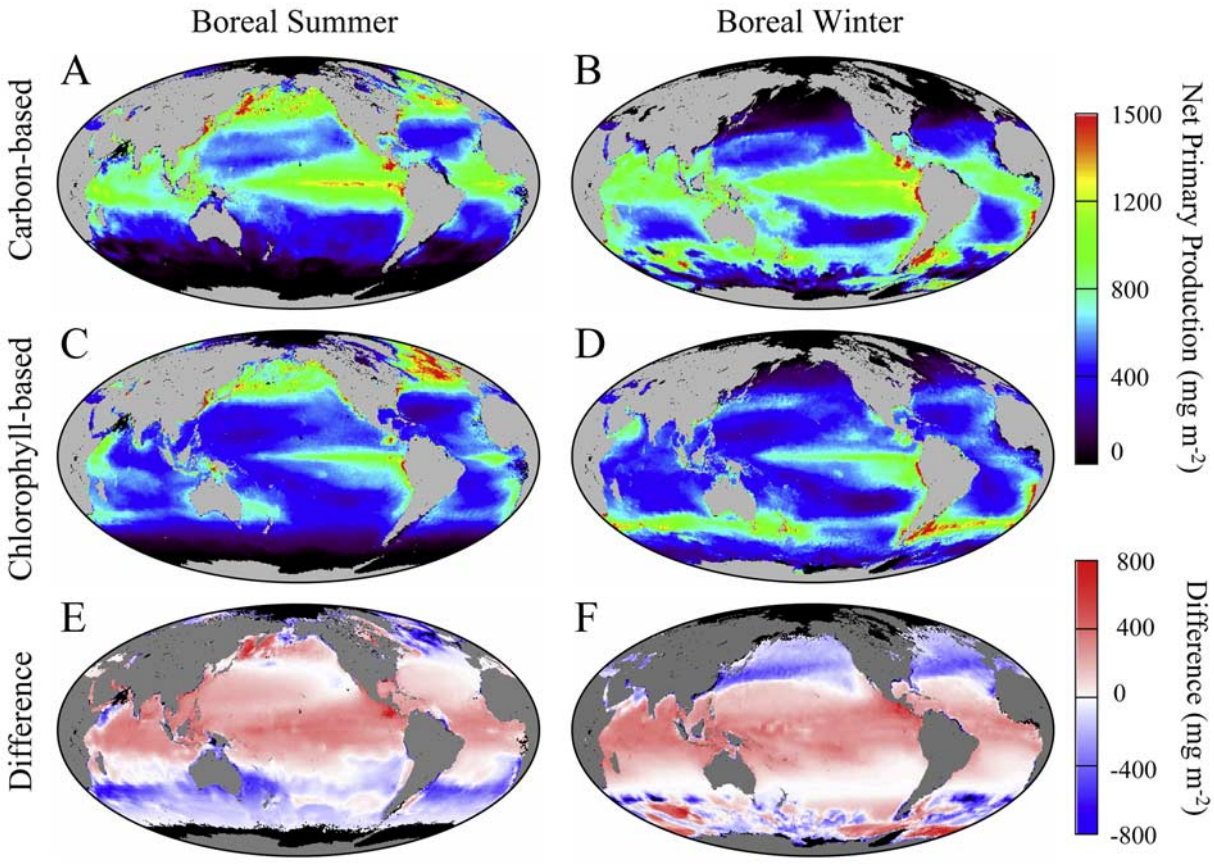

Figure 5. Seasonal mean water column net primary production (mg C m^2 d^{-1}) calculated from (a, b) satellite phytoplankton carbon and growth rate estimates and (c, d) a conventional chlorophyll-based model (the VGPM). The difference between these model NPP estimates (Figure 5e = Figure 5a – Figure 5c; Figure 5f = Figure 5b – Figure 5d) has significant implications on regional carbon cycling. (a, c, e) Boreal summer (June to August). (b, d, f) Boreal winter (December to February).

cycles in higher variance regions (see the NPP figures in the auxiliary material).

[29] When viewed by ocean basin (i.e., combining all variance levels), the C model typically gave stronger seasonal cycles in NPP at high latitudes (Figures 6a, 6c, 6d, and 6f) and persistently higher NPP at tropical latitudes (Figures 6b, 6e, and 6g). For the North Indian region, the C model indicated enhanced NPP (0.21–0.25 Pg C $month^{-1}$) in the spring (March to late May) and fall (October–December), while the Chl model yielded only a single peak (0.16 Pg C $month^{-1}$) between September and November (Figure 6g). Both models gave similar magnitude (0.8 to 1.0 Pg C $month^{-1}$), single-peaked annual cycles in NPP for the South Indian region, but the C-based cycle was offset later by roughly 2 months (Figure 6h). The two models also gave similar magnitude midsummer maxima in NPP (0.4 to 0.5 Pg C $month^{-1}$) and nearly identical fall declines for the North and South Atlantic, but summer highs for the C model were slower to develop and more sharply peaked than the broad maxima given by the Chl model (Figures 6a and 6d). A similar delay in the time of the spring bloom was also indicated for the Southern Ocean by the C model (Figure 6i). In contrast, timing of the seasonal cycle and annual integrated production were similar for the two models in the North Pacific, but the C model gave a 25% higher summer peak (0.96 Pg C $month^{-1}$) and 27% lower winter minimum (0.12 Pg C $month^{-1}$) in NPP than the Chl model (Figure 6d). In all northern and southern regions of the Atlantic and Pacific and in the Southern Ocean, the C-based model gave lower winter minima in NPP than the Chl-based model (Figures 6a, 6c, 6d, and 6f).

4. Discussion

[30] Quantification of areal net primary production from a limited set of surface observations has been a long-standing quest that can arguably be said to have roots in a 1957 paper by John H. Ryther and Charles S. Yentsch [*Ryther and Yentsch*, 1957]. In that seminal contribution, NPP was related to the product of chlorophyll biomass, daily integrated surface solar radiation, an average extinction coefficient for visible light in the water column, and a constant chlorophyll-specific assimilation efficiency of 3.7 g C (g Chl $h)^{-1}$ [*Ryther and Yentsch*, 1957]. In their

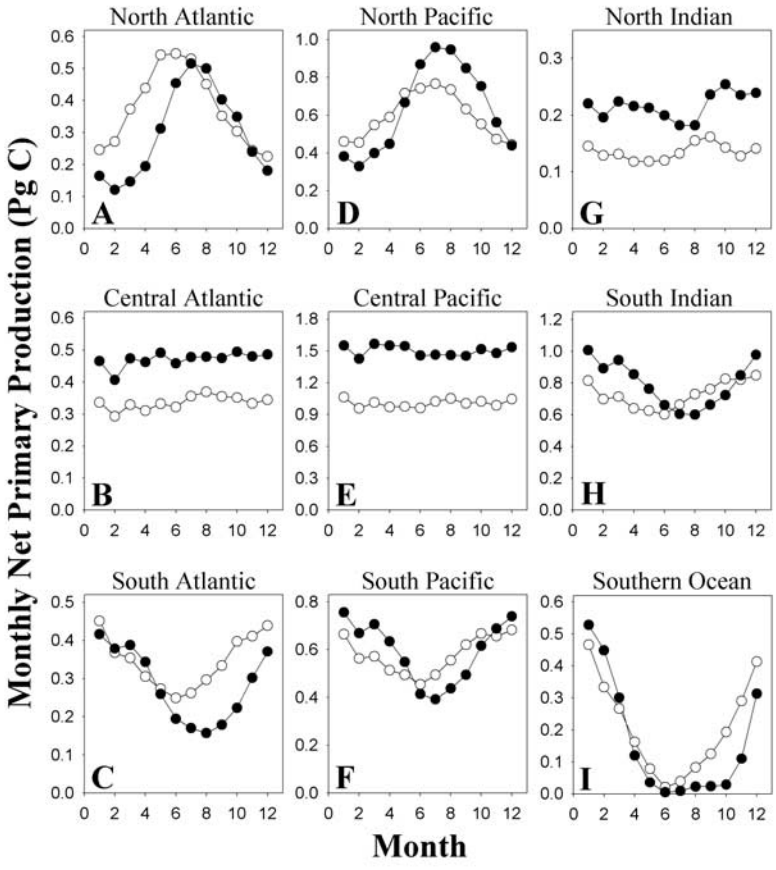

Figure 6. Seasonal cycles in net primary production for the nine ocean basins (labeled at the top of each panel) identified in Figure 2a. Solid circles denote NPP calculated from satellite phytoplankton carbon and growth rate estimates. Open circles denote NPP calculated using a conventional chlorophyll-based model (the VGPM). Seasonal cycles are based on monthly averages for the 1997 to 2002 period. Data were combined for all chlorophyll variance bins within a given ocean basin. Full temporal patterns in carbon-based and chlorophyll-based NPP for each of the 28 regional bins are provided in the NPP figures in the auxiliary material.

approach, which has been progressively developed and expanded upon ever since, chlorophyll functioned as a measure of phytoplankton biomass. An attractive aspect of chlorophyll is that it is uniquely associated with plant material, while a critical drawback is that its relation to carbon is strongly influenced by the physiological state of the phytoplankton assemblage. This later dependency is expressed as changes in the assimilation efficiency and its importance was already recognized by *Ryther and Yentsch* [1957, p. 285]: ''Probably the weakest point in the foregoing treatment is the photosynthesis-chlorophyll factor. There is little reason to assume that this must be constant under all conditions ….'' While these authors proposed potential regulating factors for the ''photosynthesis-chlorophyll'' term (i.e., temperature, light, species composition, season, and time of day), a clear path for globally modeling or remotely observing variability in chlorophyll-specific photosynthesis has even to this day never been identified. Indeed, contemporary physiological descriptions employed in satellite NPP algorithms exhibit little improvement over the assumption of a constant assimilation efficiency [*Siegel et al.*, 2001; *Campbell et al.*, 2002; *Behrenfeld et al.*, 2002].

[31] Here we propose an alternative to chlorophyll-based NPP modeling that builds upon recent field-based evidence that scattering:chlorophyll ratios track changes in phytoplankton physiology [*Behrenfeld and Boss*, 2003]. A particularly attractive aspect of this new approach is that each of the four primary variables in the NPP equation (5) can now be linked to satellite observations. This closure is achieved by associating the variable component of b_{bp} to changes in the abundance of particles functionally associated with (thus correlated to) phytoplankton carbon biomass. Strong support for this proposition is provided by the ecologically coherent temporal patterns found in Chl, C, and Chl:C ratios for our 28 regions (Figure 2 and the REGPAT figures in auxiliary material) and by the remarkable agreement between laboratory- and satellite-based

dependencies of Chl:C on light, temperature, and nutrient stress (Figure 3).

[32] An important point emphasized by our results is that chlorophyll concentration is a poor proxy of phytoplankton biomass within large areas of the ocean. Particularly in low-biomass oligotrophic regions, chlorophyll variability can be dominated by, if not exclusively due to, adjustments in physiological state (i.e., changes in Chl:C resulting from changes in growth conditions). This decoupling between phytoplankton biomass and pigmentation has been indicated in the vertical dimension of the water column [e.g., *Kiefer and Kremer*, 1981; *Kitchen and Zaneveld*, 1990; *Mitchell and Kiefer*, 1988; *Mitchell and Holm-Hansen*, 1991; *Fennel and Boss*, 2003] and here is simply extended on a global scale to the horizontal dimension. In both the vertical and horizontal dimensions, however, the physiological underpinning for this independent behavior in carbon and chlorophyll biomass is the same: acclimation to changing light, nutrient, and temperature conditions.

[33] The link between satellite Chl:C and phytoplankton physiology established here has benefited from a variety of factors. For example, excluding optically complex coastal regions and integrating open ocean data over large time (monthly) and space (regional) scales undoubtedly helps remove local-scale variability in the b_{bp}:C ratio. The wide range of growth conditions in the global oceans also helps create a dynamic range in Chl:C that is sufficient to overcome optically based changes in the b_{bp} to phytoplankton C relationship. Perhaps the most important factor, though, is the apparent compositional stability of natural particle assemblages. Indeed, field studies suggest that over seasonal cycles [*DuRand et al.*, 2001] and across oligotrophic to eutrophic conditions [*Oubelkheir*, 2001] phytoplankton contribute a relatively consistent fraction to POC, although exceptions to this rule certainly exist. For the planktonic contributors to b_{bp}, this relationship may be particularly tight because the rapid potential growth rates of the heterotrophic component allow for a close correspondence between their biomass and phytoplankton abundance.

[34] The quest to quantify areal net primary production over regional to global scales is certainly not over yet, but our results suggest that an important step has been taken in this direction. Already, the carbon-based approach has revealed some unexpected and fascinating temporal patterns in regional NPP (Figure 6, and the NPP figures in the auxiliary material) and raised important questions regarding the functioning of planktonic communities. One particularly intriguing observation has been the bilinear relationship between Chl and b_{bp} (Figure 1). This pattern suggests that at least at the regional scale, a minimum exists to which the heterotrophic community is ''willing'' to graze the phytoplankton [*Lessard and Murrell*, 1998]. Is there an energetic justification for this apparent ''floor'' in phytoplankton abundance? If not, what is the basis for this ''hinge-point'' between physiologically dominated and biomass-dominated systems? Another interesting observation has been the organization of regional Chl, C, and Chl:C data into five basic temporal patterns (Figure 2). Are these patterns simply due to ocean circulation and other physical constraints, or are they also associated with dominant ecosystem modes? Certainly, there is much left to be done here and much left to learn.

4.1. Future Directions

[35] A multitude of future research needs and exciting potential applications emerge with this first indication of a space-based optical index of phytoplankton physiology. Clearly of foremost importance is the continued development and validation of derived satellite products, including b_{bp}, phytoplankton pigment and carbon biomass, μ, and NPP. These developments will require new field measurements (as there is currently a paucity of such data) and an evolution in satellite ocean color technology that allows better separation of optically active in-water constituents (e.g., utilizing ultraviolet wave bands to better separate phytoplankton and colored dissolved organic material absorption) and improved atmospheric corrections (e.g., characterization of absorbing aerosol column thickness and heights).

[36] Improvements in the carbon-based approach can also be made in the many steps leading from satellite Chl and b_{bp} to NPP. For example, in (3) we assume that nutrient-dependent changes in Chl:C are paralleled by equivalent changes in μ. However, laboratory studies indicate that when $\mu = 0$ division d^{-1}, Chl:C is > 0. In addition, we have not yet considered potential taxonomic influences on the relationship between Chl:C and μ, nor have we attempted to adjust the b_{bp} to phytoplankton carbon relationship to account for changes in particle size distributions (often associated with features such as high-latitude spring diatom blooms) or the occurrence of high concentrations of inorganic particles (e.g., coccoliths, suspended sediments). Calculations of NPP might also benefit from expanding the current depth-integrated model (5) into a time-, depth-, and wavelength-resolved model. Relating μ to phytoplankton absorption:C rather than Chl:C may also be worthwhile, as the former is physiologically more relevant and absorption is operationally closer to ocean color than chlorophyll. Alternative relationships between Chl:C and μ might additionally be considered for physiologically unique growth conditions, such as in iron-limited high-nutrient, low-chlorophyll (HNLC) waters.

[37] One of the simplifying assumptions in our current estimates of μ from Chl:C is that surface phytoplankton assemblages are in a state of balanced growth; that is, all cellular constituents (particularly carbon and chlorophyll) are in a fully acclimated state (i.e., growing at the same rate). This assumption allows the use of basic physiological expressions and may very well be valid for the large spatial and temporal scales considered here. However, when physical perturbations to mixed layer growth conditions occur on timescales similar to or shorter than timescales of acclimation, transient episodes of unbalanced growth can ensue. Under such conditions, relationships between Chl:C and μ become complicated and can require more complex ''dynamic'' physiological models [e.g., *Geider et al.*, 1998; *Flynn*, 2001; *Flynn et al.*, 2001] to unravel. This issue of accounting for balanced versus unbalanced growth will be one of the challenges faced in extending the carbon-based approach to smaller space (<1 km^2) and time (daily) scales.

[38] A potentially important application for our phytoplankton carbon biomass and growth rate data, beyond quantifying ocean production and detecting its change, is for the development of prognostic ocean circulation-ecosystem models (i.e., ''coupled models''). In such models, phytoplankton carbon (or nitrogen) biomass and growth rates are primary derived variables. In the past, no remote sensing data have been available to directly test modeled growth rate fields, and broad assumptions have been necessary regarding Chl:C ratios (often assumed constant) to compare modeled phytoplankton carbon biomass with satellite chlorophyll data. It will now be possible with the new carbon-based approach to directly compare satellite and model estimates of phytoplankton carbon biomass and growth rates.

4.2. Perspective

[39] Photosynthesis is the primary conduit through which inorganic carbon enters the living components of the biosphere. In addition to linking ecosystem and biogeochemical processes, terrestrial and ocean productivity is functionally dependent on climate and is thus an indicator of temporal change in environmental forcings. Remote sensing is a route through which prohibitive space-time gaps in surface measurements of photosynthesis can be overcome; but photosynthesis is not directly amenable to satellite detection. For the oceans, empirical conversion factors employed to relate satellite data products (i.e., chlorophyll) to production have entailed such large uncertainties that any hope of detecting global change has been compromised.

[40] Here we present a path for retrieving the ''missing piece'' of the productivity equation from space. Our approach is rooted in well-developed physiological dependencies on light, nutrients, and temperature and in a solid understanding of the light scattering and absorption properties of ocean waters. Our resultant carbon-based NPP estimates provide a dramatically different view of how ocean productivity is distributed over space and time and point to the importance of this new development. With future improvements in ocean color remote sensing (i.e., expanded wave bands, improved atmospheric corrections) and algorithm development, the full potential of this carbon-based approach will be realized and, through the resultant closure on the productivity equation, NPP estimates will be achieved with higher fidelity and an improved capacity for detecting real trends in global ocean carbon cycling.

[41] **Acknowledgments.** This research was supported by the National Aeronautics and Space Administration (RTOP622-52-58, NAS5-00196, NAS5-00200, NAG5-12400) and the National Science Foundation (NSF-INT99-02240, OCE-0241614). We thank Karl Banse, Phil Boyd, and Vanessa Sherlock for very helpful comments and discussions, Stéphane Maritorena for remote sensing data, and Elizabeth Tollefson for support.

References

Antoine, D., J.-M. André, and A. Morel (1996), Oceanic primary production: 2. Estimation at global scale from satellite (coastal zone color scanner) chlorophyll, *Global Biogeochem. Cycles*, *10*, 57–69.

Babin, M., A. Morel, V. Fournier-Sicre, F. Fell, and D. Stramski (2003), Light scattering properties of marine particles in coastal and open ocean waters as related to the particle mass concentration, *Limnol. Oceanogr.*, *48*, 843–859.

Bader, H. (1970), The hyperbolic distribution of particle sizes, *J. Geophys. Res.*, *75*, 2822–2830.

Banse, K. (1991), Rates of phytoplankton cell division in the field and in iron enrichment experiments, *Limnol. Oceanogr.*, *36*, 1886–1898.

Behrenfeld, M. J., and E. Boss (2003), The beam attenuation to chlorophyll ratio: An optical index of phytoplankton physiology in the surface ocean?, *Deep Sea Res., Part I*, *50*, 1537–1549.

Behrenfeld, M. J., and P. G. Falkowski (1997a), Photosynthetic rates derived from satellite-based chlorophyll concentration, *Limnol. Oceanogr.*, *42*, 1–20.

Behrenfeld, M. J., and P. G. Falkowski (1997b), A consumer's guide to phytoplankton primary productivity models, *Limnol. Oceanogr.*, *42*, 1479–1491.

Behrenfeld, M. J., et al. (2001), Biospheric primary production during an ENSO transition, *Science*, *291*, 2594–2597.

Behrenfeld, M. J., E. Marañón, D. A. Siegel, and S. B. Hooker (2002), A photoacclimation and nutrient based model of light-saturated photosynthesis for quantifying oceanic primary production, *Mar. Ecol. Prog. Ser.*, *228*, 103–117.

Bishop, J. K. B. (1999), Transmissometer measurements of POC, *Deep Sea Res., Part I*, *46*, 353–369.

Bishop, J. K. B., S. E. Calvert, and M. Y. S. Soon (1999), Spatial and temporal variability of POC in the northeast Subarctic Pacific, *Deep Sea Res., Part II*, *46*, 2699–2733.

Boyd, P. W., et al. (1996), In vitro iron enrichment experiments in the NE Subarctic Pacific, *Mar. Ecol. Prog. Ser.*, *136*, 179–196.

Boyd, P., J. LaRoche, M. Gall, R. Frew, and R. M. L. McKay (1999), The role of iron, light, and silicate in controlling algal biomass in sub-Antarctic waters southeast of New Zealand, *J. Geophys. Res.*, *104*, 13,395–13,404.

Campbell, J., et al. (2002), Comparison of algorithms for estimating primary productivity from surface chlorophyll, temperature and irradiance, *Global Biogeochem. Cycles*, *16*(3), 1035, doi:10.1029/2001GB001444.

Chavez, F. P., et al. (1999), Biological and chemical response of the equatorial Pacific Ocean to the 1997–98 El Niño, *Science*, *286*, 2126–2131.

Cho, B. C., and F. Azam (1990), Biogeochemical significance of bacterial biomass in the ocean's euphotic zone, *Mar. Ecol. Prog. Ser.*, *63*, 253–259.

Claustre, H., A. Morel, M. Babin, C. Cailliau, D. Marie, J.-C. Marty, D. Tailliez, and D. Vaulot (1999), Variability in particle attenuation and chlorophyll fluorescence in the tropical Pacific: Scales, patterns, and biogeochemical implications, *J. Geophys. Res.*, *104*, 3401–3422.

Cloern, J. E., C. Grenz, and L. Vidergar-Lucas (1995), An empirical model of the phytoplankton chlorophyll/carbon ratio—The conversion factor between productivity and growth rate, *Limnol. Oceanogr.*, *40*, 1313–1321.

Doney, S. C., D. M. Glover, S. J. McCue, and F. Montserrat (2003), Mesoscale variability of Sea-viewing Wide Field-of-view Sensor (SeaWiFS) satellite ocean color: Global patterns and spatial scales, *J. Geophys. Res.*, *108*(C2), 3024, doi:10.1029/2001JC000843.

DuRand, M. D., R. J. Olson, and S. W. Chisholm (2001), Phytoplankton population dynamics at the Bermuda Atlantic Time-series station in the Sargasso Sea, *Deep Sea Res., Part II*, *48*, 1983–2003.

Eppley, R. W., F. P. Chavez, and R. T. Barber (1992), Standing stocks of particulate carbon and nitrogen in the equatorial Pacific at 150°W, *J. Geophys. Res.*, *97*, 655–661.

Esaias, W. E., R. L. Iverson, and K. Turpie (1999), Ocean province classification using ocean colour data: Observing biological signatures of variations in physical dynamics, *Global Change Biol.*, *6*, 39–55.

Fennel, K., and E. Boss (2003), Subsurface maxima of phytoplankton and chlorophyll: Steady state solutions from a simple model, *Limnol. Oceanogr.*, *48*, 1521–1534.

Flynn, K. J. (2001), A mechanistic model for describing dynamic multi-nutrient, light, temperature interactions in phytoplankton, *J. Plankton Res.*, *23*, 977–997.

Flynn, K. J., H. Marshall, and R. J. Geider (2001), A comparison of two N-irradiance interaction models of phytoplankton growth, *Limnol. Oceanogr.*, *46*, 1794–1802.

Gardner, W. D., I. D. Walsh, and M. J. Richardson (1993), Biophysical forcing on particle production and distribution during a spring bloom in the North Atlantic, *Deep Sea Res., Part II*, *40*, 171–195.

Gardner, W. D., S. P. Chung, M. J. Richardson, and I. D. Walsh (1995), The oceanic mixed-layer pump, *Deep Sea Res., Part II*, *42*, 757–775.

Garver, S. A., and D. A. Siegel (1997), Inherent optical property inversion of ocean color spectra and its biogeochemical interpretation: I. Time series from the Sargasso Sea, *J. Geophys. Res.*, *102*, 18,607–18,625.

Geider, R. J. (1987), Light and temperature dependence of the carbon to chlorophyll ratio in microalgae and cyanobacteria: Implications for physiology and growth of phytoplankton, *New Phytol.*, *106*, 1–34.

Geider, R. J., H. L. MacIntyre, and T. Kana (1998), A dynamic regulatory model of phytoplanktonic acclimation to light, nutrients, and temperature, *Limnol. Oceanogr.*, *43*, 679–694.

Gundersen, K., K. M. Orcutt, D. A. Purdie, A. F. Michaels, and A. H. Knap (2001), Particulate organic carbon mass distribution at the Bermuda Atlantic time-series Study (BATS) site, *Deep Sea Res., Part II*, *48*, 1697–1718.

Harrison, P. J., et al. (1999), Comparison of factors controlling phytoplankton productivity in the NE and NW subarctic Pacific, *Prog. Oceanogr.*, *43*, 205–234.

Kamykowski, D., S.-J. Zentara, J. M. Morrison, and A. C. Switzer (2002), Dynamic global patterns of nitrate, phosphate, silicate, and iron availability and phytoplankton community composition from remote sensing data, *Global Biogeochem. Cycles*, *16*(4), 1077, doi:10.1029/2001GB001640.

Kiefer, D. A., and J. Berwald (1992), A random encounter model for the microbial planktonic community, *Limnol. Oceanogr.*, *37*, 457–467.

Kiefer, D. A., and J. N. Kremer (1981), Origins of the vertical patterns of phytoplankton and nutrients in the temperate, open ocean: A stratigraphic hypothesis, *Deep Sea Res.*, *28*, 1087–1105.

Kitchen, J., and J. R. Zaneveld (1990), On the noncorrelation of the vertical structure of light scattering and chlorophyll *a* in case I waters, *J. Geophys. Res.*, *95*, 20,237–20,246.

Laws, E. A., and T. T. Bannister (1980), Nutrient- and light-limited growth of *Thalassiosira fluviatilis* in continuous culture, with implications for phytoplankton growth in the ocean, *Limnol. Oceanogr.*, *25*, 457–473.

Lessard, E. J., and M. C. Murrell (1998), Microzooplankton herbivory and phytoplankton growth in the northwestern Sargasso Sea, *Aquat. Microbial Ecol.*, *16*, 173–188.

Lindley, S. T., R. R. Bidigare, and R. T. Barber (1995), Phytoplankton photosynthesis parameters along 140°W in the equatorial Pacific, *Deep Sea Res., Part II*, *42*, 441–463.

Loisel, H., and A. Morel (1998), Light scattering and chlorophyll concentration in case 1 waters: A reexamination, *Limnol. Oceanogr.*, *43*, 847–858.

Loisel, H., E. Bosc, D. Stramski, K. Oubelkheir, and P.-Y. Deschamps (2001), Seasonal variability of the backscattering coefficient in the Mediterranean Sea on Satellite SeaWiFS imagery, *Geophys. Res. Lett.*, *28*, 4203–4206.

Longhurst, A. (1995), Seasonal cycles of pelagic production and consumption, *Prog. Oceanogr.*, *36*, 77–167.

MacIntyre, H. L., T. M. Kana, T. Anning, and R. J. Geider (2002), Photoacclimation of photosynthesis irradiance response curves and photosynthetic pigments in microalgae and cyanobacteria, *J. Phycol.*, *38*, 17–38.

Maritorena, S., D. A. Siegel, and A. R. Peterson (2002), Optimization of a semianalytical ocean color model for global-scale applications, *Appl. Opt.*, *41*, 2705–2714.

McClain, C. R., S. R. Signorini, and J. R. Christian (2004), Subtropical gyre variability observed by ocean-color satellites, *Deep Sea Res., Part II*, *51*, 281–301.

Mitchell, B. G., and O. Holm-Hansen (1991), Bio-optical properties of Antarctic Peninsula waters: Differentiation from temperate ocean models, *Deep Sea Res.*, *38*, 1009–1028.

Mitchell, B. G., and D. A. Kiefer (1988), Variability in pigment specific particulate fluorescence and absorption spectra in the northeastern Pacific Ocean, *Deep Sea Res.*, *35*, 665–689.

Morel, A., and Y.-H. Ahn (1991), Optics of heterotrophic nanoflagellates and ciliates: A tentative assessment of their scattering role in oceanic waters compared to those of bacterial and algal cells, *J. Mar. Res.*, *48*, 1–26.

Oubelkheir, K. (2001), Biogeochemical characterization of various oceanic provinces through optical indicators over various space and time scales, Ph.D. thesis, 216 pp., Univ. de la Méditer./CNRS, Marseille, France.

Ryther, J. H., and C. S. Yentsch (1957), The estimation of phytoplankton production in the ocean from chlorophyll and light data, *Limnol. Oceanogr.*, *2*, 281–286.

Sakshaug, E., K. Andresen, and D. A. Kiefer (1989), A steady state description of growth and light absorption in the marine planktonic diatom *Skeletonema costatum*, *Limnol. Oceanogr.*, *34*, 198–205.

Siegel, D. A., et al. (2001), Bio-optical modeling of primary production on regional scales: The Bermuda BioOptics project, *Deep Sea Res., Part II*, *48*, 1865–1896.

Siegel, D. A., et al. (2002), Global distribution and dynamics of colored dissolved and detrital organic materials, *J. Geophys. Res.*, *107*(C12), 3228, doi:10.1029/2001JC000965.

Stramski, D., and D. A. Kiefer (1991), Light scattering by microorganisms in the open ocean, *Prog. Oceanogr.*, *28*, 343–383.

Stramski, D., R. A. Reynolds, M. Kahru, and B. G. Mitchell (1999), Estimation of particulate organic carbon in the ocean from satellite remote sensing, *Science*, *285*, 239–242.

Sullivan, C. W., K. R. Arrigo, C. R. McClain, J. C. Comiso, and J. Firestone (1993), Distributions of phytoplankton blooms in the Southern Ocean, *Science*, *262*, 1832–1837.

Switzer, A. C., D. Kamykowski, and S.-J. Zentara (2003), Mapping nitrate in the global ocean using remotely sensed sea surface temperature, *J. Geophys. Res.*, *108*(C8), 3280, doi:10.1029/2000JC000444.

Twardowski, M. S., E. Boss, J. B. Macdonald, W. S. Pegau, A. H. Barnard, and J. R. Zaneveld (2001), A model for estimating bulk refractive index from the optical backscattering ratio and the implications for understanding particle composition in case I and case II waters, *J. Geophys. Res.*, *106*, 14,129–14,142.

Walsh, I. D., S. P. Chung, M. J. Richardson, and W. D. Gardner (1995), The diel cycle in the integrated particle load in the equatorial Pacific: A comparison with primary production, *Deep Sea Res., Part II*, *42*, 465–477.

Winn, C. D., L. Campbell, J. R. Christian, R. M. Letelier, D. V. Hebel, J. E. Dore, L. Fujieki, and D. M. Karl (1995), Seasonal variability in the phytoplankton community of the North Pacific Subtropical Gyre, *Global Biogeochem. Cycles*, *9*, 605–620.

M. J. Behrenfeld, Department of Botany and Plant Pathology, Oregon State University, Cordley Hall, 2082, Corvallis, OR 97331, USA. (behrenfm@science.oregonstate.edu)

E. Boss, School of Marine Sciences, 209 Libby Hall, University of Maine, Orono, ME 04469-5741, USA. (emmanuel.boss@maine.edu)

D. M. Shea, Science Applications International Corporation, NASA Goddard Space Flight Center, Greenbelt, MD 20771, USA. (don.shea@gsfc.nasa.gov)

D. A. Siegel, Institute for Computational Earth System Science, University of California, Santa Barbara, Santa Barbara, CA 93106-3060, USA. (davey@icess.ucsb.edu)